In Situ Monitoring Mesoscopic Deformation of Nanostructured Porous Titania Films Caused by Water Ingression

Lin Song,[a,b] *Monika Rawolle,*[b] *Nuri Hohn,*[b] *Jochen S. Gutmann,*[c] *Henrich Frielinghaus,*[d] *and Peter Müller-Buschbaum**[b,e].

[a]Xi'an Institute of Flexible Electronics (IFE), Northwestern Polytechnical University (NPU), Xi'an 710072, Shaanxi, China.

[b]Lehrstuhl für funktionelle Materialien, Physik Department, Technische Universität München. James-Franck-Str. 1, 85748 Garching, Germany. E-mail: muellerb@ph.tum.de

[c]Fakultät für Chemie, Physikalische Chemie, Universität Duisburg-Essen, Universitätsstr. 5, 45141, Essen, Germany.

[d]Jülich Center for Neutron Science (JCNS) at Heinz Maier-Leibnitz Zentrum (MLZ), Forschungszentrum Jülich GmbH, Lichtenbergstr. 1, 85748 Garching, Germany.

[e]Heinz Maier-Leibnitz Zentrum (MLZ), Technische Universität München, Lichtenbergstr. 1, 85748 Garching, Germany.

KEYWORDS

mesoporous TiO_2, D_2O ingression, mesoscopic deformation, elastic modulus, in situ GISANS

ABSTRACT

Nanostructured porous titania films are used in many energy related applications. In this work, the temporal evolution of the mesoscopic deformation of mesoporous titania films synthesized via block copolymer assisted sol-gel chemistry is investigated with in situ grazing incidence small-angle neutron scattering (GISANS) during exposure to D_2O vapor. Two types of mesoporous titania films are compared, which have a different degree of structural stability, depending on the applied annealing temperature (400 °C versus 600 °C) in nitrogen atmosphere. Water ingression causes a gradual structure deformation in terms of decreasing center-to-center distances and broadening of the size distribution of the titania nanostructures. Based on the evolution of the mesopore size obtained from in situ GISANS measurements, the results show that structures synthesized at lower temperature undergo a stronger deformation due to the lower elastic modulus originating from larger pores, despite having a higher degree of order.

1. INTRODUCTION

Mesoporous titania thin films with a large surface-to-volume ratio have showed great promise in applications of water splitting, degradation of organic pollutants, hydrogen storage, dye-sensitized solar cells and lithium batteries.[1-6] In the context of these energy applications, it is often necessary to infiltrate the mesoporous titania films with liquid during processing or during operation. Prominent examples are water entering the titania network in water splitting applications or aqueous solutions of small molecules being used for dye adsorption or for backfilling in dye-sensitized solar cells. In such scenarios, the capillary pressure within the mesopores induced by liquid permeation can cause a potentially irreversible deformation of the titania nanostructures.[7-9] However, only few research groups have investigated the change of the nanostructured titania films, even though structural changes have a crucial impact on the practical applications. In particular, irreversible changes would cause deviations from the titania nanostructure being present in the devices from an initially tailor-made titanai nanostructure with potentially optimized characteristic length scales.

Structural deformation of mesoporous solids has been reported to play an important role in the performance of nanopore-featured functional materials and devices. For example, Han et al. demonstrated that the plastic deformation of a nanoporous silica gel at a high-pressure resulted in a higher energy absorption efficiency.[10] Zhao et al. showed a fast and large-shape deformation of a porous polymer membrane upon the exposure to water and acetone vapor, which gave an ultra-fast actuation speed in terms of the response rate and the amplitude of movement.[11] Boudot et al. developed a humidity-driven actuator based on adsorption-induced deformation of mesoporous and xerogel-based silica thin films. [12] Quinn and McIntosh demonstrated that water adsorption caused a higher degree of elastic deformation of porous glass than butane adsorption, which was attributed to the difference in surface tension.[13] Recently, we studied the water induced deformation of titania nanostructures as function of the applied annealing atmosphere during the sol-gel synthesis of the mesoporous titania network structure and identified a nitrogen atmosphere to be superior to an air atmosphere.[14]

In view of the significance of the structural deformation on material and/or device performance, the detailed understanding of the temporal evolution of the deformation in real time is of particular interest. However, in situ experiments studying these processes are quite rare. Among the examples from the literature, Prass et al. applied in situ x-ray diffraction to measure the strain of ordered nanoporous silica as function of the relative vapor pressure of different fluids, from which elastic moduli of the porous silica were extracted.[15] Balzer et al. performed in situ dilatometric measurements to characterize the length variation of rod-like porous materials in response to adsorption-induced strains.[16] However, these approaches only revealed the macroscopic deformation of the measured materials in real time. Since adsorption behavior occurs inside the mesopores, in situ characterization, which focuses on the nano/mesoscale deformation, is considered to be highly valuable. Nevertheless, to the best of our knowledge, such a characterization does not yet exist.

In the present work, we use in situ grazing incidence small-angle neutron scattering (GISANS) measurements to track the temporal evolution of the mesoscopic deformation occurring in mesoporous titania thin films upon water ingression for the first time. Compared to real space imaging techniques like atomic force microscopy (AFM) and scanning electron microscopy (SEM), GISANS measurements are not restricted to map surface structures but also yield access to morphological information from inside the film.[17-20] Furthermore, by probing a macroscopic area of the sample, in situ GISANS measurements provide a high statistical relevance with a reasonable time resolution to probe kinetic processes. [21-23]

Previously, we demonstrated the use of GISANS measurements to reveal the mesoscopic deformation of nanostructured titania films upon capillary forces.[14] Different atmospheres for polymer-template removal at high temperatures were used to prepare mesoporous titania films, which ultimately led to different degrees of structure deformation during the exposure to water vapor.[14] We also showed that the structure deformation was completely reversible after the removal of infiltrated water.[14] In the present work, we focus on using time resolved GISANS to unravel the kinetic evolution of the mesoscopic deformation of titania nanostructures.

Mesoporous titania films are prepared by combining sol-gel chemistry with a titania precursor and the diblock-copolymer template polydimethyl siloxane-block-methyl methacrylate polyethylene oxide (PDMS-b-MA(PEO)).[24] A high temperature process is used to remove the polymer template and to form a mesoporous morphology of an interconnected titania network.[25-28] For comparison, we investigate the evolution of the mesoscopic deformation on two types of mesoporous titania films, which are prepared with different annealing temperatures in nitrogen atmosphere. Typically, with increase of the annealing temperature, crystal sizes and crystallinity of the titania films increase correspondingly, whereas high temperatures tend to give rise to the collapse of the titania network structures and thereby lead to small pore sizes. [29-32]

2. Experimental Section

Materials: The polymer PDMS-b-MA(PEO) with the molecular weight Mn (PDMS) = 5000 g mol^{-1} and Mn (MA(PEO)) = 3000 g mol^{-1} was synthesized as explained in the literature.[60] Iso-propanol (IPA, 99.9 %), tetrahydrofuran (THF, 99.9 %), hydrochloric acid (HCl, 12 M), and titanium tetra-isopropoxide (TTIP, 97%) were obtained from Carl Roth GmbH. All chemicals were used directly without any additional purification.

Preparation of mesoporous titania films: Two types of mesoporous titania films were fabricated in this work. The procedure of the film preparation was the same except for the used annealing temperatures in the final step of the synthesis. In detail, PDMS-b-MA(PEO) (152 mg) was firstly dissolved in a solvent mixture for 30 min. This mixture consists of THF (1.92 mL) and IPA (0.72 mL). After stirring, the polymer solution was filtered with a polytetrauoroethylene (PTFE) filter (pore size 0.45 μm) prior to the addition of TTIP (80 μL) and HCl (42.6 μL). Both were added simultaneously into the polymer solution with a speed of about 2 s per a drop under constant stirring conditions. The final weight ratio in the solution was 6:3:1 of PDMS-b-MA(PEO):TTIP:HCl. The final solution was stirred for 1 h at room temperature before spin-

coated on pre-cleaned Si substrates (2000 rpm, 60 s). Finally, the as-prepared films were annealed at 400 °C or 600 °C for 4 h in a nitrogen atmosphere to remove the polymer template.

Film characterization: SEM measurements were carried out on a field emission electron microscope (FESEM, Zeiss Gemini Nvision 40). The acceleration voltage was set to 5.0 kV. At the FRM II, Heinz Maier-Leibnitz Zentrum (Garching, Germany), the in situ GISANS measurements were conducted at the small angle neutron scattering beamline KWS1 (Jülich Centre for Neutron Science, JCNS).[61] The neutron wavelength was set to λ = 4.5 Å and the incident angle was 0.55°, which enabled neutron beams to penetrate the whole volume of the probed titania films as the critical angle of titania is smaller (0.23°). Before starting the in situ GISANS measurements, the samples were placed in an custom-made aluminum chamber, which was mounted on the sample stage. An initial 5 min GISANS measurement was performed prior to D_2O injection. Thereafter, D_2O was injected to the chamber and the chamber was heated up to 40 °C gradually. For the in situ measurements in the first hour, the data acquisition time was 5 min to follow the temporal evolution. An acquisition time of 30 min was chosen for the next 4 hours during which no more changes were observed. The total measurement time accounted for 5 hours for each in situ study. The scattering signal was recorded with a 2D ^{6}Li scintillator glass detector. This detector had a pixel size of 5.25 mm × 5.25 mm and a 128 × 128 pixel array. To obtain a desirable q range, a sample-to-detector distance was set to 6.66 m.

3. RESULTS AND DISCUSSION

Figure 1 shows plan-view SEM images of mesoporous titania films after high-temperature annealing in nitrogen atmosphere at 400 °C and 600 °C, which demonstrates the extended control of the nanostructures and mesopores by varying the annealing temperature. [33] The samples annealed at 400 °C and 600 °C are denoted as *N_2-400* and *N_2-600*, respectively.

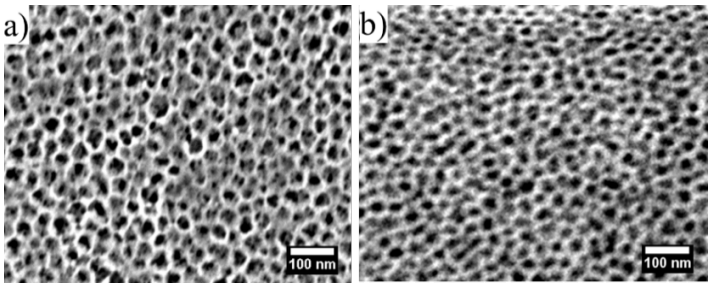

Figure 1. SEM images of a) mesoporous titania thin films (*N_2-400*) annealed at 400 °C and b) mesoporous titania thin films (*N_2-600*) annealed at 600° in nitrogen atmosphere.

Both films exhibit a titania nanomesh with high pore density. The *N2-400* sample shows a comparably more ordered mesopore array with pore sizes ranging from 20 nm to 25 nm (Figure 1a). For an annealing temperature of 600 °C, the *N_2-600* film displays a more irregular mesopore array and smaller pore sizes of 10 nm - 15 nm (Figure 1b). The differences in the degree of order and in pore size are ascribed to the different degree of film collapse as induced by the variation of the annealing temperature.[34-36] The differences in the crystallinity are discussed in the literature.[37,38]

The in situ GISANS experiments follow the D_2O ingression into the mesoporous titania films which are exposed to D_2O vapor atmosphere. The relative humidity and the temperature inside the sample chamber are shown in Figure S1 in the Supporting Information. The use of D_2O in the experiment instead of H_2O provides the necessary scattering contrast for the neutron scattering experiment. Compared to grazing incidence small-angle X-ray scattering (GISAXS) measurements, the higher scattering contrast of titania and D_2O in neutron scattering measurements allows for tracking the mesoscopic deformation kinetics of nanostructured titania films more precisely.[14] During D_2O ingression, time resolved GISANS measurements probe the temporal evolution of the mesoscopic deformation of the titania films. The entire experiment lasts for 5 h and is divided into two steps: The first hour is measured with a time resolution of 5 min to follow the initial fast changes and the remaining 4 h are measured with a time resolution

of 30 min to verify stability of the changed structure. The experimental details can be found in the Experimental Section. For the *N_2-400* film, exemplary two dimensional (2D) GISANS data after different times of exposure to D_2O vapor are displayed in Figure S2 in the Supporting Information. In order to extract information about lateral nanostructures inside the titania thin films, horizontal line cuts of the 2D GISANS data are performed at the Yoneda peak position of titania.[39] This peak is located at the critical angle of the probed material, where the material specific diffuse scattering is enhanced as described by the Fresnel transmission functions.[39] Since a major contribution to the diffuse scattering at the Yoneda peak is material characteristic, characterization of lateral structures of titania films including characteristic domain sizes and the corresponding spatial arrangement can be well realized.[40-43] Horizontal line cuts from the first hour are shown in Figure 2a.

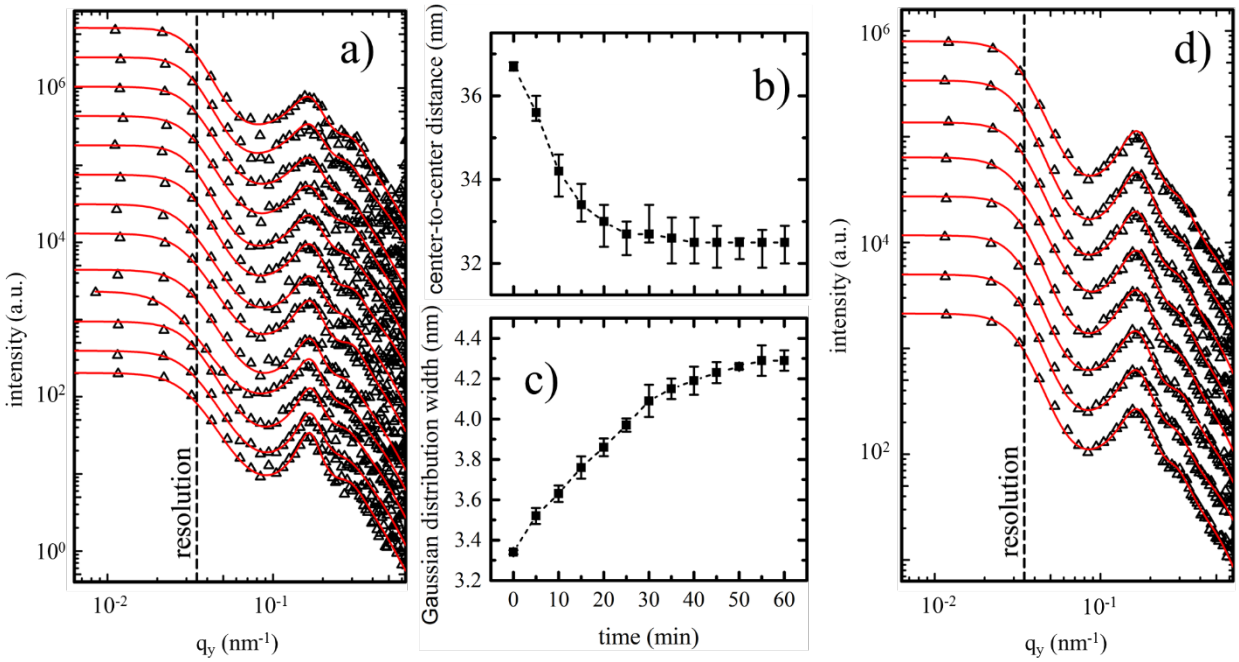

Figure 2 In situ GISANS data of the *N_2-400* film during exposure to D_2O vapor for 5 h. a) Horizontal line cuts (black hollow triangles) of the 2D GISANS data (obtained from the first hour measurements) plotted from bottom to top for increasing time. The time resolution is 5 min. The bottom curve is obtained from the measurement before D_2O injection and extracted structural information referred to as 0 min. The red lines show the fits to the data. The curves are shifted along the intensity axis for clarity of the presentation. Extracted b) center-to-center distance of the titania nanostructures and c) Gaussian distribution width as a function of exposure time. d) Horizontal line cuts (black hollow triangles) of the 2D GISANS data (obtained from the next 4 hours measurements) plotted from bottom to top for increasing time. The time resolution is 30 min. The bottom curve refers to the measurement at an exposure time of 1.5 h. The red lines show the fits to the data. The curves are shifted along the intensity axis for clarity.

A pronounced intensity peak located in the vicinity of q_y = 0.18 nm^{-1} is observed for the horizontal line cut obtained from the sample before D_2O injection, implying an ordered inner arrangement of the mesopores for the *N_2-400* film.[44-46] This observation agrees well with SEM measurements, suggesting that the ordered pore array exists not only at the sample surface but also inside the film. In addition, a slight shift of the peak position toward lower q_y values is observed (Figure 2a), suggesting a structural change of the mesoporous titania films. Moreover, the peak at q_y = 0.18 nm^{-1} is the most pronounced feature. Consequentially, nanostructures, which contribute to the scattering signal of this peak, are considered as most representatives for the inner film morphology. Thus, the peak at q_y = 0.18 nm^{-1} is chosen to parametrize the evolution of the most predominant structure deformation. However, with increasing exposure time to D_2O vapor, a gradual broadening of the peak is indicating a transition to a reduced state of mesopore array order inside the titania films. To quantitatively characterize the evolution of mesoscopic deformation for the *N2-400* film, the horizontal line cuts are modeled in the framework of the distorted wave Born approximation (DWBA), assuming two cylindrically shaped scattering objects distributed over a 1D paracrystal lattice in a manner of a so-called local monodisperse approximation (LMA). [47-50] Detailed information about data modeling is described elsewhere.[45] From data modeling, two characteristic domain sizes of titania nanostructures (form factors) and the corresponding center-to-center distances (structure factors) are extracted. The modeling results originating from the well-pronounced peak at q_y = 0.18 nm^{-1} show that the pore array has a rather high degree of order. The domain radius stays approximatively constant at 5.5 nm for all probed D_2O exposure times. Thus, the size of the titania nanostructures is not influenced by D_2O-induced capillary forces. In contrast, the extracted center-to-center distances decrease with exposure time to D_2O vapor from (36.7 ± 0.1) nm to (32.5 ± 0.5) nm after one hour as summarized in Figure 2b. It can be seen that the center-to-center distance gradually decreases during the initial 30 min of exposure, and subsequently remains stable until the end of the first

hour. The relative humidity has raised significantly faster (see Figure S1 in the Supporting Information), indicating that the center-to-center distance responds delayed on the change of the environment due to water ingression. In contrast, the Gaussian distribution widths of the intensity peak increase steadily from (3.3 ± 0.1) nm for the film before D_2O ingression to (4.3 ± 0.1) nm for the sample after exposure to D_2O vapor for 1 h (Figure 2c). The increase of the Gaussian distribution resembles the decrease in order of the pore array during water ingression. The center-to-center distance shrinks by about 11 %, whereas the Gaussian distribution width increases by approximately 31 % in the first hour, which is a clear sign that the *N_2-400* film experiences a structure deformation during exposure to D_2O vapor. Figure 2d shows the horizontal line cuts of 2D GISANS data obtained during the next four hours of D_2O exposure. As seen in the data and confirmed by modeling, the center-to-center distance (32.5 ± 0.5 nm) and the Gaussian distribution width (4.3 ± 0.1 nm) remain unchanged. Thus, after the deformation of the titania nanostructure happening in the initial one hour (Figure 2a), no further evidence for structure changes are found.

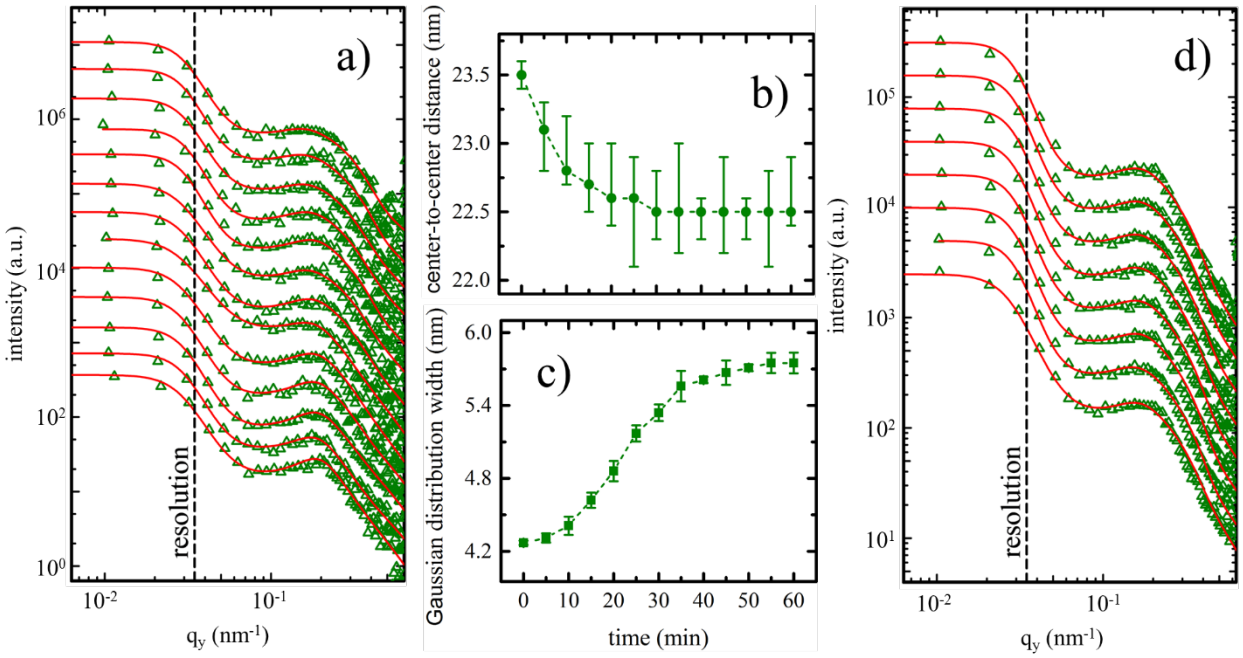

Figure 3 In situ GISANS data of the *N_2-600* film during exposure to D_2O vapor for 5 h. a) Horizontal line cuts (green hollow triangles) of the 2D GISANS data (obtained from the first hour measurements) plotted from bottom to top for increasing time. The time resolution is 5 min. The bottom curve is obtained from the measurement before D_2O injection and extracted

structural information referred to as 0 min. The red lines show the fits to the data. The curves are shifted along the intensity axis for clarity of the presentation. Extracted b) center-to-center distance of the titania nanostructures and c) Gaussian distribution width as a function of exposure time. d) Horizontal line cuts (green hollow triangles) of the 2D GISANS data (obtained from the next 4 hours measurements) plotted from bottom to top for increasing time. The time resolution is 30 min. The bottom curve refers to the measurement at an exposure time of 1.5 h. The red lines show the fits to the data. The curves are shifted along the intensity axis for clarity.

For the *N_2-600* film, selected 2D GISANS data for different times are displayed in Figure S3 in the Supporting Information. The obtained horizontal line cuts with their corresponding fits are shown in Figure 3a and 3d. Comparable to the *N_2-400* film, the domain radius stays constant for the whole time of exposure to D_2O vapor as well. However, the absolute value of the extracted domain radius of the most prominent structure is 6.5 nm and thereby slightly larger than the value for the *N2-400* film (about 5.5 nm). The evolution of the predominant center-to-center distances, which originates from the peak at $q_y \approx 0.19$ nm^{-1}, and the corresponding Gaussian distribution width have a similar tendency as for the *N_2-400* film. Consequentially, the key influence, which causes structural deformation, is the water ingression in both cases. However, the absolute values differ. For the *N_2-600* film, the center-to-center distance of (23.5 ± 0.1) nm in the initial state (no exposure to D_2O) is smaller as compared to the *N_2-400* film, while the respective Gaussian distribution width is slightly larger (4.3 ± 0.1 nm), which is in good agreement with the observations obtained from SEM measurements. With increasing exposure time to D_2O vapor, the center-to-center distance decreases by about 5 % to a value of (22.5 ± 0.4) nm (Figure 3c), whereas the Gaussian distribution width increases by 32 % to (5.8 ± 0.1) nm (Figure 3d). After one hour of exposure, both values, the center-to-center distance and the Gaussian distribution width, remain constant as well, suggesting that the time required for structure deformation of titania nanostructures is not linked to the annealing temperature applied during the synthesis of the mesoporous morphology.

The comparative analysis of both samples shows that, the evolution of the center-to-center distances of the *N_2-400* film is more susceptible to capillary-force-induced mesoscopic deformation than that of the *N_2-600* film. Additionally, the similar increase of the Gaussian

distribution width (percentage-wise) with exposure time to D_2O vapor indicates a mechanism, which reduces the lateral order of the nanostructures independent of the initial annealing temperature. The summarized parameters from in situ 2D GISANS data imply a higher degree of mesoscopic deformation of the titania nanostructures in the *N_2-400* sample. This behavior can be explained as the concentration of oxygen vacancies increases with increasing annealing temperature,[51-53] and oxygen vacancies are beneficial to strengthen the Ti-O bonds and to reduce water adsorption.[52, 54-57] Therefore, less oxygen vacancies account for more structure deformation in the *N_2-400* film.

Dourdain et al. reported a method to determine the elastic modulus of mesoporous thin films based on the degree of deformation as induced by capillary forces of water vapor.[58] In detail, the capillary pressure introduces deformation of the pores, which can be used to evaluate the strain. Along this route, the elastic modulus (E_{mod}) of the mesoporous film is defined as

$$E_{mod} = p_c/[(D - D_0)/D_0] \quad (1)$$

where p_c is the capillary pressure, D and D_0 are the distorted and original pore size, respectively. The capillary pressure p_c is related to the relative humidity (RH) as described by the Kelvin equation,

$$lnRH = p_c V_L/(\mathrm{RT}) \quad (2)$$

with the molar volume of water V_L, the gas constant R and the temperature T. Therefore, the relationship of the pore size and the elastic modulus (E_{mod}) can be described as

$$D = D_0(1 + \mathrm{RT}/(E_{mod}V_L)lnRH) \quad (3)$$

The pore size in this work is calculated following the model introduced by our previous studies[59]

$$D = center\text{-}to\text{-}center\ distance - 2\times domain\ radius \quad (4)$$

To calculate the elastic modulus according to equation (3), the obtained pore sizes for both samples are plotted as a function of Tln*RH* (Figure 4). Via a linear fitting of D versus Tln*RH*, the elastic moduli of the *N_2-400* film and the *N_2-600* film are determined to be (1.1 ± 0.1) GPa and (1.8 ± 0.1) GPa, respectively. The relatively smaller elastic modulus of the *N_2-400* film as compared to the *N_2-600* film is attributed to the reduced Ti-O bond strength, which is a result of the reduced amount of oxygen vacancies at reduced annealing temperatures and the fact that the *N_2-600* is initially already in a more compact status (smaller pore sizes of 10.5 ± 0.1 nm). Moreover, the smaller elastic modulus in turn explains the higher degree of mesoscopic deformation of the *N_2-400* film.

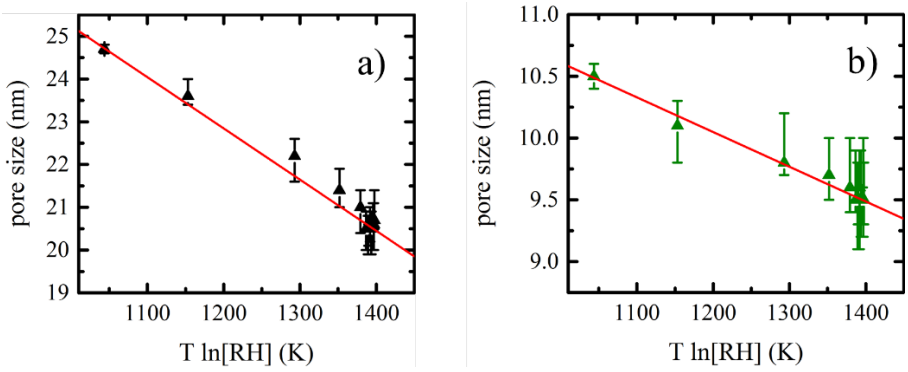

Figure 4 Evolution of the mesopore size extracted from in situ 2D GISANS data as a function of the temperature (T) times natural logarithm of the relative humidity (RH) for a) the *N_2-400* film and b) the *N_2-600* film. Red lines represent the linear fits to the data. Linear fits are used to calculate the elastic modulus of the respective samples.

4. CONCLUSION

In conclusion, we successfully monitor the mesoscopic deformation of mesoporous titania films in real time upon exposure to D_2O vapor through in situ GISANS measurements. At 400 °C as compared to 600 °C annealing temperature during synthesis of the titania nanostructures, titania films with larger pore sizes and a higher degree of order of the pore array are synthesized. The water ingression induced structure deformation manifests in the decreased center-to-center

distances of the titania nanostructures and the increased Gaussian distribution width. It mainly occurs within the first hour of water ingression and remains unchanged for the next four hours. A higher degree of structure deformation is found in the titania films synthesized at lower temperature in view of the decrease percentage of the center-to-center distances. It is caused by larger pores giving rise to a smaller elastic modulus of (1.1 ± 0.1) GPa for the *N_2-400* films as compared to (1.8 ± 0.1) GPa for the *N_2-600* films, despite the higher degree of order established at lower temperature. Thus, it is concluded that the annealing temperature plays an important role not only for the pore size and the degree of order of the pore array, but also in the mechanical stability of titania nanostructures against water adsorption. These finding will be interesting for all water based dye molecule, polymer and electrolyte solutions used in the fabrication of dye sensitized solar cells, hybrid solar cells and battery or catalysis applications. Furthermore, this work provides an efficient way to characterize the evolution of mesoscopic deformation of mesoporous structures in real time, which could be easily adapted to other mesoporous solids such as for example ZnO, SiO_2, ZrO_2.

Supporting Information.

Data plot of temperature and relative humidity during in situ GISANS measurements, 2D GISANS data of the *N_2-400* film and the *N_2-600* film can be found in the Supporting Information file.

Corresponding Author

* Email: muellerb@ph.tum.de

Notes

The authors declare no competing financial interests.

ACKNOWLEDGMENT

This work was supported by funding from TUM.solar in the context of the Bavarian Collaborative Research Project Solar Technologies Go Hybrid (SolTech), International Research Training Group 2022 Alberta/Technical University of Munich International Graduate School for Environmentally Responsible Functional Hybrid Materials (ATUMS) and by the Deutsche Forschungsgemeinschaft (DFG, German Research Foundation) under Germany's Excellence Strategy – EXC 2089/1 – 39077626 (e-conversion). L. S. was supported by "the Fundamental Research Funds for the Central Universities". The authors thank Dr. Maria D'Acunzi for synthesis of the diblock copolymer and Professor Alexander Holleitner and Peter Weiser for the access to SEM measurements.

REFERENCES

(1) Pham, T. A.; Ping, Y.; Galli, G. Modelling Heterogeneous Interfaces for Solar Water Splitting. *Nat. Mater.* **2017**, *16*, 401-408.

(2) Dong, H. R.; Zeng, G. M.; Tang, L.; Fan, C.; Zhang, C.; He, X.; He, Y. An Overview on Limitations of TiO2-based Particles for Photocatalytic Degradation of Organic Pollutants and the Corresponding Countermeasures. *Water Res.* **2015**, *79*, 128-146.

(3) Zhang, R.; Elzatahry, A. A.; Al-Deyab, S. S.; Zhao, D. Mesoporous titania: From Synthesis to Application. *Nano Today* **2012**, *7*, 344-366.

(4) Gohari-Bajestani, Z.; Akhlaghi, O.; Yurum, Y.; Yürüm, A. Synthesis of Anatase TiO2 with Exposed (001) Facets Grown on N-doped Reduced Graphene Oxide for Enhanced Hydrogen Storage. *Int. J. Hydrogen Energy* **2017**, *42*, 6096-6103.

(5) Ye, M.; Wen, X.; Wang, M.; Iocozzia, J.; Zhang, N.; Lin, C.; Lin, Z. Recent Advances in Dye-Sensitized Solar Cells: from Photoanodes, Sensitizers and Electrolytes to Counter Electrodes. *Mater Today* **2015**, *18*, 155-162.

(6) Chen, D.; Caruso, R. A. Recent Progress in the Synthesis of Spherical Titania Nanostructures and Their Applications. *Adv. Funct. Mater.* **2013**, *23*, 1356-1374.

(7) Gor, G. Y.; Huber, P.; Bernstein, N. Adsorption-Induced Deformation of Nanoporous Materials-A Review. *Appl. Phys. Rev.* **2017**, *4*, 011303.

(8) Balzer, C.; Waag, A. M.; Gehret, S.; Reichenauer, G.; Putz, F.; Hüsing, N.; Paris, O.; Bernstein, N.; Gor, G. Y.; Neimark, A. V. Adsorption-Induced Deformation of Hierarchically Structured Mesoporous Silica-Effect of Pore-Level Anisotropy. *Langmuir* **2017**, *33*, 5592-5602.

(9) Rahman, T.; Liu, R.; Ortel, E.; Kraehnert, R.; Antoniou, A. Mechanical Behavior of Mesoporous Titania Thin Films. *Appl. Phys. Lett.* **2014**, *104*, 241902.

(10) Han, A.; Punyamurthula, V. K.; Lu, W.; Qiao, Y. Deformation of a Nanoporous Silica under Compressive Loading. *J. Appl. Phys.* **2008**, *103*, 084318.

(11) Zhao, Q.; Dunlop, J. W. C.; Qiu, X.; Huang, F.; Zhang, Z.; Heyda, J.; Dzubiella, J.; Antonietti, M.; Yuan, J. An Instant Multi-Responsive Porous Polymer Actuator Driven by Solvent Molecule Sorption. *Nat. Commun.* **2014**, *5*, 4293.

(12) Boudot, M.; Elettro, H.; Grosso D. Converting Water Adsorption and Capillary Condensation in Usable Forces with Simple Porous Inorganic Thin Films. *ACS Nano* **2016**, *10*, 10031-10040.

(13) Quinn, H. W.; Mcintosh, R. The Hysteresis Loop in Adsorption Isotherms on Porous Vycor Glass and Associated Dimensional Changes of the Adsorbent. II. *Can. J. Chem.* **1957**, *35*, 745-756.

(14) Song, L.; Rawolle, M.; Hohn, N.; Gutmann, J. S.; Frielinghaus, H.; Müller-Buschbaum, P. Deformation of Mesoporous Titania Nanostructures in Contact with D2O Vapor. *Small* **2018**, *14*, 1801461.

(15) Prass, J.; Müter, D.; Fratzl, P.; Paris, O. Capillarity-Driven Deformation of Ordered Nanoporous Silica. *Appl. Phys. Lett.* **2009**, *95*, 083121.

(16) Balzer, C.; Wildhage, T.; Braxmeier, S.; Reichenauer, G.; Olivier, J. P. Deformation of Porous Carbons upon Adsorption. *Langmuir* **2011**, *27*, 2553-2560.

(17) Rawolle, M.; Sarkar, K.; Niedermeier, M. A.; Schindler, M.; Lellig, P.; Gutmann, J. S.; Moulin, J. F.; Haese-Seiller, M.; Wochnik, A. S.; Scheu, C.; Müller-Buschbaum, P. Infiltration of Polymer Hole-Conductor into Mesoporous Titania Structures for Solid-State Dye-Sensitized Solar Cells. *ACS Appl. Mater. Interface* **2013**, *5*, 719-729.

(18) Nouhi, S.; Hellsing, M. S.; Kapaklis, V.; Rennie, A. R. Grazing-Incidence Small-Angle Neutron Scattering from Structures below an Interface. *J. Appl. Crystallogr.* **2017**, *50*, 1066-1074.

(19) Hexemer, A.; Müller-Buschbaum, P. Advanced Grazing-Incidence Techniques for Modern Soft-Matter Materials Analysis. *IUCrJ* **2015**, *2*, 106-125.

(20) Adlmann, F. A.; Herbel, J.; Korolkovas, A.; Bliersbach, A.; Toperverg, B.; Van Herck, W.; Pálsson, G. K.; Kitchen, B.; Wolff, M. Depth Resolved Grazing Incidence Neutron Scattering Experiments from Semi-Infinite Interfaces: a Statistical Analysis of the Scattering Contributions. *J. Phys.: Condens. Mat.* **2018**, *30*, 165901.

(21) Salditt, T.; Brotons, G. Biomolecular and Amphiphilic Films Probed by Surface Sensitive X-ray and Neutron Scattering. *Anal. Bioanal. Chem.* **2004**, *379*, 960-973.

(22) Jaksch, S.; Lipfert, F.; Koutsioubas, A.; Mattauch, S.; Holderer, O.; Ivanova, O.; Frielinghaus, H.; Hertrich, S.; Fischer, S. F.; Nickel, B. Influence of Ibuprofen on Phospholipid Membranes. *Phys. Rev. E* **2015**, *91*, 022716.

(23) Förster, S.; Timmann, A.; Konrad, M.; Schellbach, C.; Meyer, A.; Funari, S. S.; Mulvaney, P.; Knott. R. Scattering Curves of Ordered Mesoscopic Materials. *J. Phys. Chem. B* **2005**, *109*, 1347-1360.

(24) Rawolle, M.; Ruderer, M. A.; Prams, S. M.; Zhong, Q.; Magerl, D.; Perlich, J.; Roth, S. V.; Lellig, P.; Gutmann, J. S.; Müller-Buschbaum, P. Nanostructuring of Titania Thin Films by a Ccombination of Microfluidics and Block-Copolymer-Based Sol-Gel Templating. *Small* **2011**, *7*, 884-891.

(25) Guldin, S.; Kolle, M.; Stefik, M.; Langford, R.; Eder, D.; Wiesner, U.; Steiner, U. Tunable Mesoporous Bragg Reflectors Based on Block-Copolymer Self-Assembly. *Adv Mater.* **2011**, *23*, 3664-3668.

(26) Song, L.; Wang, W.; Pröller, S.; Moseguí González, D.; Schlipf, J.; Schaffer, C. J.; Peters, K.; Herzig, E. M.; Bernstorff, S.; Bein, T.; Fattakhova-Rohlfing, D.; Müller-Buschbaum, P. In Situ Study of Degradation in P3HT-Titania-Based Solid-State Dye-Sensitized Solar Cells. *ACS Energy Lett.* **2017**, *2*, 991-997.

(27) Fischer, M. G.; Hua, X.; Wilts, B. D.; Gunkel, I.; Bennett, T. M.; Steiner, U. Mesoporous Titania Microspheres with Highly Tunable Pores as an Anode Material for Lithium Ion Batteries. *ACS Appl. Mater. Interface* **2017**, *9*, 22388-22397.

(28) Lokupitiya, H. N.; Jones, A.; Reid, B.; Guldin, S.; Stefik, M. Ordered Mesoporous to Macroporous Oxides with Tunable Isomorphic Architectures: Solution Criteria for Persistent Micelle Templates. *Chem. Mater.* **2016**, *28*, 1653-1667.

(29) Catauro, M.; Tranquillo, E.; Dal Poggetto, G.; Pasquali, M.; Dell'Era, A.; Vecchio Ciprioti, S. Influence of the Heat Treatment on the Particles Size and on the Crystalline Phase of TiO2 Synthesized by the Sol-Gel Method. *Materials* **2018**, *11*, 2364.

(30) Khan, M. A.; Shaheer Akhtar, M.; Yang, O-B. Synthesis, Characterization and Application of Sol-Gel Derived Mesoporous TiO2 Nanoparticles for Dye-Sensitized Solar Cells. *Solar Energy* **2010**, *84*, 2195-2201.

(31) Yu, J.; Yu, J. C.; Leung, M. K.-P.; Ho, W.; Cheng, B.; Zhao, X.; Zhao, J. Effects of Acidic and Basic Hydrolysis Catalysts on the Photocatalytic Activity and Microstructures of Bimodal Mesoporous Titania. *J. Catal.* **2003**, *217*, 69-78.

(32) Mechiakh, R.; Sedrine, N. B.; Chtourou, R.; Bensaha, R. Correlation between Microstructure and Optical Properties of Nano-Crystalline TiO2 Thin Films Prepared by Sol-Gel Dip Coating. *Appl. Surf. Sci.* **2010**, *257*, 670-676.

(33) Rawolle, M.; Niedermeier, M. A.; Kaune, G.; Perlich, J.; Lellig, P.; Memesa, M.; Cheng, Y.-J.; Gutmann, J. S.; Müller-Buschbaum, P. Fabrication and Characterization of Nanostructured Titania Films with Integrated Function from Inorganic-Organic Hybrid Materials. *Chem. Soc. Rev.* **2012**, *41*, 5131-5142.

(34) Cao, L.; Chen, D. H.; Li, W.; Caruso, R. A. Hierarchically Porous Titania Networks with Tunable Anatase: Rutile Ratios and Their Enhanced Photocatalytic Activities. *ACS Appl. Mater. Interface* **2014**, *6*, 13129-13137.

(35) Shiba, K.; Sato, S.; Matsushita, T.; Ogawa, M. Preparation of Nanoporous Titania Spherical Nanoparticles. *J. Solid State Chem.* **2013**, *199*, 317-325.

(36) Choi, S. Y.; Mamak, M.; Speakman, S.; Chopra, N.; Ozin, G. A. Evolution of Nanocrystallinity in Periodic Mesoporous Anatase Thin Films. *Small* **2005**, *1*, 226-232.

(37) Fattakhova-Rohlfing, D.; Wark, M.; Brezesinski, T.; Smarsly, B. M.; Rathouský, J. Highly Organized Mesoporous TiO2 Films with Controlled Crystallinity: A Li-Insertion Study. *Adv. Funct. Mater.* **2007**, *17*, 123-132.

(38) Smarsly, B.; Grosso, D.; Brezesinski, T.; Pinna, N.; Boissière, C.; Antonietti, M.; Sanchez, C. Highly Crystalline Cubic Mesoporous TiO2 with 10-nm Pore Diameter Made with a New Block Copolymer Template. *Chem. Mater.* **2004**, *16*, 2948-2952.

(39) Yoneda, Y. Anomalous Surface Reflection of X Rays. *Phys. Rev.* **1963**, *131*, 2010-2013.

(40) Song, L.; Wang, W. J.; Körstgens, V.; Moseguí González, D.; Yao, Y.; Minar, N. K.; Feckl, J. M.; Peters, K.; Bein, T.; Fattakhova-Rohlfing, D.; Santoro, G.; Roth, S. V.; Müller-Buschbaum, P. Spray Deposition of Titania Films with Incorporated Crystalline Nanoparticles for All-Solid-State Dye-Sensitized Solar Cells Using P3HT. *Adv. Funct. Mater.* **2016**, *26*, 1498-1506.

(41) Paik, M. Y.; Bosworth, J. K.; Smilges, D. M.; Schwartz, E. L.; Andre, X.; Ober, C. K. Reversible Morphology Control in Block Copolymer Films via Solvent Vapor Processing: An in Situ GISAXS Study. *Macromolecules* **2010**, *43*, 4253-4260.

(42) Lupi, F. F.; Giammaria, T. J.; Seguini, G.; Laus, M.; Dubcek, P.; Pivac, B.; Bernstorff, S.; Perego, M. GISAXS Analysis of the In-Depth Morphology of Thick PS-b-PMMA Films. *ACS Appl. Mater. Interface* **2017**, *9*, 11054-11063.

(43) Martin, D. J.; Decarolis, D.; Odarchenko, Y. I.; Herbert, J. J.; Arnold, T.; Rawle, J.; Nicklin, C.; Boyen, H. G.; Beale, A. M. Reversible Restructuring of Supported Au Nanoparticles during Butadiene Hydrogenation Revealed by Operando GISAXS/GIWAXS. *Chem. Commun.* **2017**, *53*, 5159-5162.

(44) Lin, Y.; Böker, A.; He, J.; Sill, K.; Xiang, H.; Abetz, C.; Li, X.; Wang, J.; Emrick, T.; Long, S.; Wang, Q.; Balazs, A.; Russell, T. P. GISAXS Analysis of the In-Depth Morphology of Thick PS-b-PMMA Films. *Nature* **2005**, *434*, 55-59.

(45) Song, L.; Wang, W. J.; Körstgens, V.; Moseguí González, D.; Löhrer, F. C.; Schaffer, C. J.; Schlipf, J.; Peters, K.; Bein, T.; Fattakhova-Rohlfing, D.; Roth, S. V.; Müller-Buschbaum, P. In Situ Study of Spray Deposited Titania Photoanodes for Scalable Fabrication of Solid-State Dye-Sensitized Solar Cells. *Nano Energy* **2017**, *40*, 317-326.

(46) Samant, S.; Strzalka, J.; Yager, K. G.; Kisslinger, K.; Grolman, D.; Basutkar, M.; Salunke, N.; Singh, G.; Berry, B.; Karim, A. Ordering Pathway of Block Copolymers under Dynamic Thermal Gradients Studied by in Situ GISAXS. *Macromolecules* **2016**, *49*, 8633-8642.

(47) Rauscher, M.; Paniago, R.; Metzger, H.; Kovats, Z.; Domke, J.; Peisl, J.; Pfannes, H. D.; Schulze, J.; Eisele, I. Grazing Incidence Small Angle x-ray Scattering from Free-Standing Nanostructures. *J. Appl. Phys.* **1999**, *86*, 6763-6769.

(48) Pedersen, J. S. Determination of Size Distribution from Small-Angle Scattering Data for Systems with Effective Hard-Sphere Interactions. *J. Appl. Crystallogr.* **1994**, *27*, 595-608.

(49) Renaud, G.; Lazzari, R.; Leroy, F. Probing Surface and Interface Morphology with Grazing Incidence Small Angle X-Ray Scattering. *Surf. Sci. Rep..* **2009**, *64*, 255-380.

(50) Li, T.; Senesi, A. J.; Lee, B. Small Angle X-ray Scattering for Nanoparticle Research. *Chem. Rev.* **2016**, *116*, 11128-11180.

(51) Wang, K.; Chang, Y.; Lv, L.; Long, Y. Effect of Annealing Temperature on Oxygen Vacancy Concentrations of Nanocrystalline CeO2 Film. *Appl. Surf. Sci.* **2015**, *351*, 164-168.

(52) Morgan, B. J.; Watson, G. W. Intrinsic n-Type Defect Formation in TiO2: A Comparison of Rutile and Anatase from GGA+U Calculations. *J. Phys. Chem. C.* **2010**, *114*, 2321-2328.

(53) An, X.; Hu, C.; Liu, H.; Qu, J. Effect of Annealing Temperature on Oxygen Vacancy Concentrations of Nanocrystalline CeO2 Film. *Langmuir* **2018**, *34*, 1883-1889.

(54) Janotti, A.; Varley, J. B.; Rinke, P.; Umezawa, N.; Kresse, G.; Van de Walle, C. G. Hybrid Functional Studies of the Oxygen Vacancy in TiO2. *Phys. Rev. B* **2010**, *81*, 085212.

(55) Naldoni, A.; Allieta, M.; Santangelo, S.; Marelli, M.; Fabbri, F.; Cappelli, S.; Bianchi, C. L.; Psaro, R.; Dal Santo, V. Effect of Nature and Location of Defects on Bandgap Narrowing in Black TiO2 Nanoparticles. *J. Am. Chem. Soc.* **2012**, 1*34*, 7600-7603.

(56) Hugenschmidt, M. B.; Gamble, L.; Campbell, C. T. The Interaction of H2O with a TiO2(110) Surface. *Surf. Sci.* **1994**, *302*, 329-340.

(57) Henderson, M. A. Structural Sensitivity in the Dissociation of Water on TiO2 Single-Crystal Surfaces. *Langmuir* **1996**, *12*, 5093-5098.

(58) Dourdain, S.; Britton, D. T.; Reichert, H.; Gibaud, A. Determination of the Elastic Modulus of Mesoporous Silica thin Films by x-ray Reflectivity via the Capillary Condensation of Water. *Appl. Phys. Lett.* **2008**, *93*, 183108.

(59) Song, L.; Abdelsamie, A.; Schaffer, C. J.; Körstgens, V.;. Wang, W. J; Wang, T. Y.; Indari, E. D.; Fröschl, T.; Hüsing, N.; Haeberle, T.; Lugli, P.; Bernstorff, S.; Müller-Buschbaum, P. A Low Temperature Route toward Hierarchically Structured Titania Films for Thin Hybrid Solar Cells. *Adv. Funct. Mater.* **2016**, *26*, 7084-7093.

(60) Kaune, G.; Memesa, M.; Meier, R.; Ruderer, M. A.; Diethert, A.; Roth, S. V.; D'Acunzi, M.; Gutmann, J. S.; Müller-Buschbaum, P. Hierarchically Structured Titania Films Prepared by Polymer/Colloidal Templating. *ACS Appl. Mater. Interface* **2009**, *1*, 2862-2869.

(61) Feoktystov, A. V.; Frielinghaus, H.; Di, Z. Y.; Jaksch, S.; Pipich, V.; Appavou, M. S.; Babcock, E.; Hanslik, R.; Engels, R.; Kemmerling, G.; Kleines, H.; Ioffe, A.; Richter, D.; Brückel, T. KWS-1 High-Resolution Small-Angle Neutron Scattering Instrument at JCNS: Current State. *J. Appl. Crystallogr.* **2015**, *48*, 61-70.

TOC